Key Engineering Materials Vol. 454 (2011) pp 47-77
Online available since 2010/Dec/06 at www.scientific.net

doi:10.4028/www.scientific.net/KEM.454.47

Boundary element analysis of three-dimensional interface cracks in transversely isotropic bimaterials using the Energy Domain Integral

N.O. Larrosa[1,3], J.E. Ortiz[2] and A.P. Cisilino[3,a]

[1] Escuela Superior de Ingenieros, Escuela Superior de Ingenieros, Universidad de Sevilla. Av. de los Descubrimientos s/n, E-41092, Sevilla, España.

[2] Departamento de Mecánica de Medios Continuos, Escuela Superior de Ingenieros, Universidad de Sevilla. Av. de los Descubrimientos s/n, E-41092, Sevilla, España.

[3] División Soldadura y Fractomecánica, INTEMA. Facultad de Ingeniería, Universidad Nacional de Mar del Plata – CONICET, Av. Juan B. Justo 4302, B7608FDQ, Mar del Plata, Argentina.
[a] cisilino@fi.mdp.edu.ar

Keywords: three-dimensional interface cracks, transversely isotropic bimaterials, energy domain integral, boundary element method.

Abstract

It is presented in this paper a three-dimensional Boundary Element Method (BEM) implementation of the Energy Domain Integral for the fracture mechanical analysis of three-dimensional interface cracks in transversely isotropic bimaterials. The *J*-integral is evaluated using a domain representation naturally compatible with the BEM, in which the stresses, strains and derivatives of displacements at internal points are evaluated using their appropriate boundary integral equations. Several examples are solved and the results compared with those available in the literature to demonstrate the efficiency and accuracy of the implementation to solve straight and curved crack-front problems.

1 Introduction

The greatest advantage of composite materials is strength and stiffness combined with lightness. By choosing an appropriate combination of reinforcement and matrix material, manufacturers can produce materials with mechanical properties that fit the requirements for a particular structure for a particular purpose.

Commonly, high strength and stiffness are required in various directions within a plane. The solution is to stack and weld together a number of plies, each having the fibres oriented in different directions. Such a stack is termed a laminate. The individual plies present a macroscopic transversely isotropic behaviour with the symmetry axis in the direction of the fibres (Gibson, 2007).

Delamination is one of the most important damage mechanisms in laminate composites. It consists in the nucleation of interface cracks between the plies of the laminate as consequence of thermo-mechanical fatigue, impact or material degradation (Gibson, 2007). Once cracking initiation has arisen, preventing crack growth (propagation) is the variable to control in order the keep the material in a reliable condition. It is therefore important to develop fracture-mechanics methods for assessing interface cracks and predicting their

behaviour during the material life time.

Many questions regarding the mechanics of interface fracture have been answered during the past few decades. However, progress has been generally focused in the two-dimensional idealization of an interface crack, and not until recently major effort has been conducted on the three-dimensional aspect of interface fracture. This is in part due to the complexity of such problems and the very large computational efforts required for their numerical analysis. However, given the material mismatch at the interface boundary, it is expected that the three-dimensional effects play a more significant role in a laminate structure than in a homogenous structure.

The numerical analysis of interface cracks in transversally isotropic materials has been traditionally addressed using Finite Element Analysis (FEA) (see for example Boniface and Banks-Sills, 2002 and Freed and Banks-Sills, 2005). Besides, there is the alternative of using the Boundary Element Method (BEM). The attraction of the BEM can be largely attributed to the reduction in the dimensionality of the problem; for two-dimensional problems, only the line-boundary of the domain needs to be discretized into elements, and for three-dimensional problems only the surface of the domain needs to be discretized. This means that, compared to finite-element domain-type analysis, a boundary analysis results in a substantial reduction in data preparation. At the same time, and due to the inherent characteristics of its formulation, BEM provides very accurate results for problems containing strong geometrical discontinuities. This makes BEM a powerful numerical tool for modelling crack problems (see Aliabadi, 1997). Fracture mechanical analysis of three dimensional transversely isotropic materials using BEM has been reported by Sáez et al. (1997) and Ariza and Dominguez (2004a, 2004b) who modelled static and dynamic crack problems, Zhao et al. (1998) who derived the displacement discontinuity boundary integral equation, and more recently by Chen et al. (2009) who studied the stress intensity factors of a central square crack in a transversely isotropic cuboid with arbitrary material orientations. To our knowledge, there is no published material about the three dimensional BEM modelling of interface cracks in dissimilar transversely isotropic bimaterials.

A number of techniques have been proposed for the evaluation of fracture parameters of interface cracks using FEM and BEM. They are, among others, the virtual crack extension approach (So, Lau and Ng; 2004), contour and domain path-independent integrals (Chow and Atluri, 1998; Ortiz and Cisilino, 2005; Freed and Banks-Sills, 2005; Shah, Tan and Wang, 2006), displacement extrapolation techniques (Freed and Banks-Sills, 2005; Tan and Gao, 1990; Mao and Sun, 1995) and special crack-tip elements (He, Lin and Ding, 1994). In particular, path-independent integral techniques are derived from the *J*-integral proposed by Rice (1968). Being an energy approach, path-independent integrals eliminate the need to solve local crack tip fields accurately. If the integration domain is defined over a relatively large portion of the mesh, an accurate modelling of the crack tip is unnecessary because the crack tip field contribution to the overall energy is not significant. At the same time, it is worth noting that the *J*-integral as it was developed by Rice (1968) characterizes the crack driving force for two-dimensional problems. Therefore, for general three-dimensional cases involving cracks of arbitrary shape an alternative form for the *J*-integral is needed.

Three basic schemes have evolved for the numerical computation of the *J*-integral in three dimensions: virtual crack extension methods, generalization of Rice's contour integral, and domain integral methods (Anderson, 1994). Domain integrals are equivalent to the virtual crack extension technique and are better suited for numerical analysis than contour integral methods. Among the available domain integral methods

(see for example Nikishkov and Atluri ,1987 and Saliva et al, 2000) the Energy Domain Integral (EDI) due to Moran and Shih (1987) was chosen for this work.

The EDI can be formulated by applying the divergence theorem to Rice's *J*-integral. It produces a domain independent integral defined over finite volumes enclosing some portion of the crack front (Moran and Shih, 1987). Previous works by the authors of this paper have demonstrated the versatility and efficiency of the BEM implementation of the EDI for assessing three-dimensional cracks in elastic (Cisilino et al, 1998), elastoplastic (Cisilino and Aliabadi, 1999) and thermoelastic bodies (Balderrama et al, 2006 and 2008) and for interface cracks in dissimilar isotropic bimaterials (Ortiz and Cisilino, 2005).

It is presented in this work the BEM implementation of the EDI for the *J*-integral computation in three-dimensional interface cracks in dissimilar transversely isotropic bimaterials. The BEM solution strategy for the fracture problem and the EDI implementation is an extension of that proposed by Ortiz and Cisilino (2005) for interface cracks in dissimilar isotropic bimaterials. A number of examples demonstrate the suitability of the proposed numerical tool for assessing delamination cracks in composite laminates.

2 Transversely isotropic materials

The basic constitutive expressions governing the elastic behaviour of transversely isotropic materials are reviewed next following Ting (1996).

The general constitutive law of the anisotropic material is

$$\sigma_{ij}(x) = C_{ijkl}(x)\varepsilon_{kl}(x) = C_{ijkl}(x)u_{k,l}(x) \tag{1}$$

where $\sigma_{ij}(x)$ is the stress tensor, $\varepsilon_{ij}(x)$ is the infinitesimal strain tensor and $u_k(x)$ is the displacement vector. Partial derivatives are indicated using the comma notation. The symbol $C_{ijkl}(x)$ is the fourth-order constitutive tensor which is defined in terms of 21 independent elasticity constants.

Transversely isotropic materials are those with an axis of symmetry such that all directions perpendicular to that axis are on a plane of isotropy. In such a case the constitutive tensor can be defined in terms of 5 independent elasticity constants only. Using the Voight reduced notation (see Ting, 1996), the fourth-order constitutive tensor C_{ij} $(i,j = 1,\dots,6)$ for a transversely isotropic material with the axis of symmetry coincident with the Cartesian axis x_3 can be expressed in terms of the five following elastic constants:

$$C_{1111} = C_{11},\ C_{3333} = C_{33},\ C_{1122} = C_{12},\ C_{1133} = C_{13} \text{ and } C_{2323} = C_{44}\ . \tag{2}$$

Due to the symmetry with respect to x_3, $C_{66} = (C_{11} - C_{12})/2$.

The coefficients of the constitutive tensor C_{ij} can be written in terms of the elastic engineering constants as follows:

$$C_{11} = \frac{E(n - v'^2)}{\lambda(1+v)},\ C_{12} = \frac{E(n + v'^2)}{\lambda(1+v)}, C_{13} = \frac{Ev'}{\lambda},\ C_{33} = \frac{E(1+v)}{\lambda}, C_{44} = \mu', \tag{3}$$

being:

$$\lambda = n(1-v) - 2v'^2 \text{ and } n = E/E', \tag{4}$$

where

- E and E' are the Young's moduli in the plane of isotropy and in the directions normal to it, respectively.
- ν is the Poisson's ratio that represents the strain response in the plane of isotropy due to an action parallel to it; and ν' is the lateral strain response for the planes normal to the plane of isotropy.
- μ' is the shear modulus for the planes normal to the planes of transverse isotropy.

3 Elastic solution in the vicinity of 3D interface crack front

Consider a three-dimensional crack front with a continuously turning tangent as depicted in Figure 1*a*. Define a local coordinate system x^* at position η, where the crack energy release rate is evaluated, given by x_1^* normal to the crack front, x_2^* normal to the crack plane, and x_3^* tangent to the crack front.

The elastic solution at the neighbourhood of the interface crack front can be expressed using a double series expansion of the form:

$$u(r,\theta,\eta) = \sum_{i\geq 1}\sum_{j\geq 0} \partial_3^j K_i(\eta) r^{\alpha_i+j} \varphi_j^{(\alpha_i)}(\theta), \tag{5}$$

for $Re(\alpha_p) \leq Re(\alpha_q)$ when $p < q$. The symbol u in equation (5) is the displacement vector in cylindrical coordinates (see Figure 1*a*), $K_i(\eta)$ is the Stress Intensity Factor (SIF) associated to exponent α_i, and $\varphi_j^{(\alpha_i)}(\theta)$ is an angular function. The exponent and the angular function depend of the boundary conditions over the crack faces, solids angles of the materials and the material properties (see Omer and Yosibash, 2008).

When $j = 0$ in equation (5), α_i and $\varphi_0^{(\alpha_i)}(\theta)$ yield the solution for the two-dimensional crack problem. For a crack in a homogenous material $\alpha_1 = \alpha_2 = \alpha_3 = 1/2$, $\alpha_4 = 1$ and the coefficients K_i are the well-known stress intensity factors (SIFs) K_{I}, K_{II} and K_{III}, respectively. For interface cracks the exponents α_i are complex numbers where $Re(\alpha_1) = Re(\alpha_2) = Re(\alpha_3) = 1/2$ and $Re(\alpha_4) = 1$. The additional high order terms in Eq. (5) when $j \geq 1$ are the so-called "shadow terms" not present in the two dimensional problem. The shadow terms are originated by variation of the SIFs along the crack front.

4 The energy domain integral

Following Natha and Moran (1993), the energy release rate, $G(\eta)$, due to crack extension in its own plane along a three-dimensional crack front takes the form (see Figure 1*b*)

$$G(\eta) = \lim_{C\to 0} \xi_k(\eta) \int_{C(\eta)} \left(w \cdot \delta_{ki} - \sigma_{ij}^* u_{j,k}^*\right) n_i dC, \tag{6}$$

where w is the strain energy density, $\boldsymbol{\sigma_{ij}^*}$ and $\boldsymbol{u_{j,k}^*}$ are Cartesian components of stress and displacement derivatives expressed in the system $\boldsymbol{x}^*$, $\boldsymbol{\xi_k(\eta)}$ are the components of the unit outward normal to the crack front in the crack plane $\boldsymbol{x_1^* - x_3^*}$, $\boldsymbol{n_i}$ is the unit vector normal to the contour $\boldsymbol{C(\eta)}$ (which lies in the $\boldsymbol{x_1^* - x_2^*}$ plane), and $\boldsymbol{dC}$ is the differential of the arc length $\boldsymbol{C}$. It is worth noting that, although Eq. (6) comes from a two-dimensional analysis, it applies for a general three-dimensional case. This is because the three-dimensional stress field along a crack front of arbitrary shape is the same to that governing a two-dimensional plain strain problem (see Omer and Yosibash, 2008). Thus, the energy domain integral introduced in this section can be used for the solution of cracks of arbitrary shape in three-dimensions.

In order to derive the equivalent domain representation of Eq. (6), we consider a small segment $\boldsymbol{L_c}$ of the crack front that lies in the $\boldsymbol{x_1^* - x_3^*}$ plane as shown in Fig. 1*b*. Next we assume that the segment undergoes a virtual crack advance in the plane of the crack, and we define the magnitude of the advance at each point $\boldsymbol{\eta}$ as $\boldsymbol{\Delta a(\eta)}$. Note that $\boldsymbol{\Delta a(\eta)}$ varies continuously along $\boldsymbol{L_c}$ and it vanishes at each end of the segment. Now let

$$\bar{G}(\eta) = \int_{L_c} G(\eta)\Delta a(\eta) d\eta, \tag{7}$$

where $\boldsymbol{G(\eta)}$ is the integral defined in Eq.(6). When $\boldsymbol{G(\eta)}$ belongs to the point-wise energy release rate, $\boldsymbol{\bar{G}}$ gives the total energy released when the finite segment $\boldsymbol{L_c}$ undergoes the virtual crack advance.

The appropriate domain form of the point-wise crack-tip contour integral can be obtained from Eq. (7) by considering a tubular domain $\boldsymbol{V}$ surrounding the crack segment (see Figure 2). As it shown in the figure, the surface $\boldsymbol{S_t}$ is formed by translating the contour $\boldsymbol{C}$ along the segment $\boldsymbol{L_c}$, and $\boldsymbol{S_0}$ stands for the outer surface of $\boldsymbol{V}$ including the ends. Next an auxiliary vector function $\boldsymbol{q}$ is introduced, which is sufficiently smooth in $\boldsymbol{V}$ and it is defined on the surfaces of $\boldsymbol{V}$ as follows:

$$q_k = \begin{cases} \Delta a(\eta) \cdot \xi_k(\eta) \text{ on } S_t \\ 0 \text{ on } S_0 \end{cases} \tag{8}$$

Finally, in the limit as the tubular surface $\boldsymbol{S_t}$ is shrunk onto the crack segment $\boldsymbol{L_c}$ and in the absence of crack face tractions, we obtain the domain integral:

$$\bar{G}(\eta) = \int_V \left(\sigma_{ij}^* u_{j,k}^* - w \cdot \delta_{ki}\right) q_{k,i} dV. \tag{9}$$

In absence of body forces the integral $\boldsymbol{\bar{G}}$ given in Eq. (9) reduces to the domain representation of the familiar *J*-integral. If it is assumed that $\boldsymbol{G(\eta)}$ is constant along $\boldsymbol{L_c}$, it follows directly from Eq. (7) that:

$$J(\eta) = G(\eta) = \frac{\bar{G}}{\int_{L_c} \Delta a(\eta) d\eta}. \tag{10}$$

5 Boundary Element Analysis

In order to account for the non homogeneous material properties, a multi-domain BEM formulation is used for the problem solution. The modelling strategy is illustrated in the schematic representation in Figure 3, for a model consisting of two subdomains, $\Omega_I(x)$ and $\Omega_{II}(x)$, with external boundaries $\Gamma_I(x)$ and $\Gamma_{II}(x)$, respectively. Both subdomains share a common interface $\Gamma_{I-II}(x)$, a portion of which is debonded and thus an interface crack is introduced. The subdomains possess a linear transversely isotropic material behaviour as it has been described in Section 2. The orientation of the material is specified using a local Cartesian system (x_1^0, x_2^0, x_3^0) for each subdomain. In every case the direction of the symmetry axis of the material is chosen coincident with the direction x_3^0 (see Figure 3). In this way, it is possible to model interface cracks lying between laminates with arbitrary relative fibre orientations.

The standard BEM uses the displacement boundary integral equation to relate the displacement and traction fields, $u(x)$ and $t(x)$ over the model boundary in the global coordinate system (see Aliabadi, 2002):

$$c_{ik}(x')u_i(x') + \int_\Gamma T_{ik}(x,x')u_i(x)\mathrm{d}\Gamma(x) = \int_\Gamma U_{ik}(x,x')t_i(x)\mathrm{d}\Gamma(x), \tag{11}$$

where $U_{ik}(x,x')$ and $T_{ik}(x,x')$ are the displacement and traction fundamental solutions, respectively. The fundamental solutions account for the solution of *i-th* component of the displacement and traction fields, $u_i(x)$ and $t_i(x)$, at the field point, x, due to the action of a unit load acting in the direction j at the source point, x'. The symbol c_{ik} is the so-called jump term which depends on the local geometry at the source point, x', only. There are several expressions for the fundamental solutions for a transversely isotropic materials, see for example Pan and Chou (1976) and Loloi (2000). However, these solutions could be cumbersome to implement into a BEM code because of the multiple cases they consider to account for all possible material configurations and the relative positions of the source and field points. On the other hand, Távara et al. (2008) have recently derived completely general and unique expressions valid for all possible configurations given in terms of real functions only (no difficulties with using complex functions). The solutions due to Távara et al. (2008) have been used in this work.

According to Távara et al. (2008), the displacement fundamental solutions when $x' = 0$ has the form

$$U^0(x) = \frac{1}{4\pi r}H(x), \tag{12}$$

where $r = |x|$, and the matrix $H(x)$ is the modulation function of the displacement fundamental solution. The matrix $H(x)$ is symmetric and it depends on the direction of r but not on its magnitude (see Figure 4). A relatively simple and general expression of $H(x)$ can be obtained using the auxiliary vector $\hat{x} = (r_{12}, 0, x_3^0)$, where $r_{12} = \sqrt{(x_1^0)^2 + (x_2^0)^2}$; and the triad $[n, m, \hat{x}/r]$ with $n = (c, 0, -s)$ and $m = (0, 1, 0)$ where $c = cos\,\phi = x_3^0/r$ and $s = sin\ \phi = r_{12}/r$, and the angle $0 \le \phi \le \pi$, see Figure 4. For such a coordinate system only the coefficients $H_{ii}(\hat{x})$ and $H_{13}(\hat{x})$ are non-zeros (see Appendix A). The general expression of the tensor $H(x)$ for any x can be obtained by transformation of components:

$$H_{ij}(x) = \Omega_{ik}\,\Omega_{js}H_{ks}(\hat{x}), \tag{13}$$

where the rotation matrix Ω_{ij} is

$$\Omega_{ij} = \begin{pmatrix} \cos\theta & -\sin\theta & 0 \\ \sin\theta & \cos\theta & 0 \\ 0 & 0 & 1 \end{pmatrix}. \tag{14}$$

The computation of the traction fundamental solution, $T^0(x)$, follows a similar procedure. The details can be found in Távara et al. (2008).

Finally, the fundamental solutions $U_{ik}(x)$ and $T_{ik}(x)$ have to be transformed from the local coordinate system, (x_1^0, x_2^0, x_3^0), to the global one in order to assemble the boundary integral equation (11). The fundamental solutions are transformed from the local coordinate system to the global one via the standard transformations for second order tensors (see Ting, 1996):

$$\begin{aligned} U_{ij}(x) &= a_{ik}a_{jl}U^o_{kl}(x) \\ \text{and } T_{ij}(x) &= a_{ik}a_{jl}T^o_{kl}(x), \end{aligned} \tag{15}$$

where a_{ik} is the transformation matrix.

BEM models are discretized using 9-node quadrilateral elements. Continuous elements are used everywhere in the model, except at the intersections of the interface and the crack surfaces with model surface. In such cases one- and two-side discontinuous elements are used in order to avoid common nodes at the intersections (see Figure 5). It is worth noting that, although discontinuous elements are not strictly necessary to solve most of the practical bimaterial crack problems; they have been implemented in this work in order to develop a versatile and robust discretization strategy capable of dealing with general multiple subdomain problems (including the case of more than two subdomains sharing a single edge). At the same time, the implementation remains open to introduce further extensions to account for crack propagation which could require of the automatic model remeshing.

The regular BEM integrals over continuous and discontinuous elements are evaluated using standard Gaussian quadrature. In the case of nearly singular integrals an adaptive element subdivision technique is also employed. On the other hand, the Cauchy principal value integrals and the free terms are evaluated using the rigid body motion approach (see Aliabadi, 2002). Singular integrals are computed using the variable transformation technique due to Lachat and Watson (1976).

The equation (11) is applied to each of the subdomains while considering the orientation of the material as explained before. The equilibrium, $t_I = -t_{II}$, and continuity, $u_I = u_{II}$, conditions are enforced at the nodes used to discretize the common interface Γ_{I-II}. The resultant system of equations is solved for the unknown traction and displacement nodal values after specifying the boundary conditions. It is worth noting that the implemented BEM code is not capable of detecting contact between the crack surfaces, and so, its application is restricted to open cracks only. For further details on the multi-domain BEM formulation and implementation the reader is referred to the book by Aliabadi (2002).

The computation of the *J*-integral are included in the BEM code as a post-processing procedure, and so, it could be applied to the results from a particular model at a later stage. The required stresses, strains and derivatives of displacements at internal points are directly obtained from their boundary integral representations (Aliabadi, 2002):

$$u_{i,m}(X') = \int_{\Gamma} U_{ij,m}(x,X')t_j(x)\mathrm{d}\Gamma(x) - \int_{\Gamma} T_{ij,m}(x,X')u_j(x)\mathrm{d}\Gamma(x) \tag{16}$$

where X' is the coordinate of the internal point, $U_{ij,m}(x,X')$ and $T_{ij,m}(x,X')$ are the derivatives of the fundamental displacement $U_{ij}(x,X')$ and traction $T_{ij}(x,X')$ fundamental solutions respectively (see Távara et al., 2009). The boundary Γ corresponds to that of the subdomain where the internal point X' lies on. Strains and stresses at internal points can then be easily computed using the definition of the infinitesimal strain tensor $\varepsilon_{ij} = \frac{1}{2}\left(u_{i,j} + u_{j,i}\right)$ and the constitutive relationships in equation (1).

On the other hand, the derivatives of the displacements, strains and displacements for boundary points are evaluated from the boundary displacements and tractions by means of a procedure similar to that usually used for finite elements. For further details the reader is referred to the paper by Ortiz and Cisilino (2005).

Finally, and in order to proceed with the *J*-integral computation, the resultant displacement derivatives, strains and stresses for both internal and boundary points are transformed to the local the crack-front

coordinate system (x_1^*, x_2^*, x_3^*) (see Section 4) using the standard transformation rule for second-order tensors (see Ting, 1996).

6 *J*-integral Computation

The computation of *J*-integral at any position $\boldsymbol{\eta}$ on the crack front requires of the evaluation of a volume integral within closed domains that enclose a segment of the crack front $\boldsymbol{L_c}$ (see equations 9 and 10). A natural choice here is to make $\boldsymbol{\eta}$ coincident with the element nodes on the crack front, while $\boldsymbol{L_c}$ is taken as the element or element sides at which points $\boldsymbol{\eta}$ lies (on see Figure 6). The portion of the model domain in which the volume integrals are evaluated is discretized using 27-node cells. The cells are similar to the three-dimensional finite elements and they are implemented using an isoparametric interpolation scheme, being their nodes the internal points of the BEM analysis. Thus, the values of stresses, $\boldsymbol{\sigma_{ij}^*}$, strains, $\boldsymbol{\varepsilon_{ij}^*}$, and displacements derivatives, $\boldsymbol{u_{i,m}^*}$, are interpolated by means of the cell interpolation functions, $\boldsymbol{\Psi_i}$. Besides, the boundary mesh is designed to have a web shape around the crack front in order to build the integration volumes with the shape of cylinders. This is illustrated in Figure 7, where the frontal face of the model has been partially removed to show the crack and the integration domains.

As it is depicted in Figure 6, three different cases are considered depending on whether the crack front position *M* is a mid-side node, it is shared by two elements, or it is located coincident with the external surface (surface node). If the node *M* is a mid-side node or surface node, $\boldsymbol{L_c}$ (the segment of the crack front over which the *J*-integral is computed) spans over one element, connecting nodes *M*-1, *M*, and *M*+1 and nodes *M*-2, *M*-1 and *M*, respectively. On the other hand, if *M* is a shared node, $\boldsymbol{L_c}$ spans over two elements, connecting nodes from *M*-2 to *M*+2.

The function $\boldsymbol{q}$ is defined to vary quadratically in the directions tangential and normal to the crack front. This bi-quadratic definition of $\boldsymbol{q}$ has been employed with excellent results in the computation of EDI for a variety of problems in previous works (see Cisilino et al, 1998; Cisilino and Aliabadi, 1999; Ortiz and Cisilino, 2005 and Balderrama et al., 2006 and 2008). Within this approach, and considering that the evaluation point $\boldsymbol{\eta}$ is at the middle of the crack front segment $\boldsymbol{L_c}$, and $\boldsymbol{r_0}$ is the radius of the integration domain, the function $\boldsymbol{q}$ is written as:

$$q(x^*) = \left|1 - \left(\frac{x_3^*}{\frac{L_c}{2}}\right)\right| \cdot \left[1 - \left(\frac{r}{r_0}\right)^2\right] \tag{17}$$

where $\boldsymbol{r}$ is the distance from the crack front in the $\boldsymbol{x_1^* - x_2^*}$ plane as it is depicted in Figure 1. Function $\boldsymbol{q}$ is specified at all nodes within the integration volumes. Consistent with the isoparametric formulation, the *q*-values are interpolated using

$$q = \sum_{i=1}^{27} \Psi_i Q^i, \tag{18}$$

where $\boldsymbol{\Psi_i}$ are the shape functions defined within the volume cell and $\boldsymbol{Q^i}$ are the nodal values for the *i*th node. From the definition of $\boldsymbol{q}$ (see equation 7), $\boldsymbol{Q^i = 0}$ if the *i*th node is on $\boldsymbol{S_0}$ while for nodes inside *V*, $\boldsymbol{Q^i}$ are given by interpolating between the nodal values on $\boldsymbol{L_c}$ and $\boldsymbol{S_0}$.

Following standard manipulations the derivatives of $\boldsymbol{q}$ are:

$$q_{k,j} = \sum_{i=1}^{27} \sum_{l=1}^{3} \frac{\partial \Psi_i}{\partial \zeta_l} \frac{\partial \zeta_l}{\partial x_j} Q^i, \tag{19}$$

where $\boldsymbol{\zeta_k}$ are the coordinates in the cell isoparametric space and $\boldsymbol{\partial \zeta_k / \partial x_j}$ is the Jacobian matrix of the transformation.

Finally, if Gaussian integration is used, the discretized form of expression (9) is

$$\bar{G}(\eta) = \sum_{\text{cells in } V} \sum_{p=1}^{m} \left\{ \left(\sigma_{ij}^* \, u_{j,k}^* - \sigma_{ij}^* \, \varepsilon_{ij}^* \, \delta_{ki} \right) q_{k,j} det \left(\frac{\partial x_j}{\partial \zeta_k} \right) \right\}_p w_p, \tag{20}$$

where $\boldsymbol{m}$ is the number of Gaussian points per cell, and $\boldsymbol{w_p}$ are the weighting factors.

7 Application Examples

7.1 Thick tension bimaterial plate with a centre interface crack

A thick bimaterial plate containing a through crack on the interface is considered in the first example. A schematic representation of the problem geometry, dimensions and boundary conditions are depicted in Figure 8. Model discretization is similar to that depicted in Figure 7. It consists of 658 elements and 2855 nodes. Eighteen elements are placed along the crack front, and a total of 126 elements are used in the crack discretization. Five rings of cells with normalized radii r/a = 0.1, 0.2, 0.3, 0.44 and 0.64 are accommodated around the crack front for J computations. With this purpose 648 cells and 6438 nodes are employed.

In order to validate the code and to allow comparisons with other results from the bibliography, the problem was solved first for homogeneous cases, this is, the material elastic constants and orientations were set the same for both subdomains. The first case is that of an isotropic homogeneous plate with material elastic properties E=E'=100 GPa, ν=ν'=0.3 and μ'=0.5E/(1+ν). Computed J values along the crack front are presented in Figure 9, where the origin of the normalized coordinate, z/t=0, corresponds to the specimen mid-plane (see Figure 8*b*). The reference values are those reported by Raju and Newman (1977) for a homogeneous centre cracked specimen and presented in a polynomial form by Aliabadi (1996). Since reference results are reported in terms of the mode-I stress intensity factors, K_I, they have been converted to J values using the expression (see for example Anderson, 2005)

$$J = K_I^2 / \bar{E} \tag{21}$$

where $\boldsymbol{\bar{E} = E/(1-\nu^2)}$ for the plane strain condition. It is worth mentioning that the reference results are reported in terms of stress intensity factors with an accuracy of 5%. So that, when they are converted into J values using expression (21), the error bound is increased to around 10%. The accuracy of the reference J results is indicated in Figure 9 using the error bars. Data in Figure 9 are normalized with respect to the J value for a crack in a infinite homogenous plate under plane strain condition, $\boldsymbol{J_0 = \sigma^2 \pi a / \bar{E}}$. Excellent agreement is found between the reference and computed results throughout the specimen thickness. Computed results are well within the error bounds of the reference results. Results of similar accuracy were obtained using a single-domain dual boundary element method (DBEM) in a previous work by Cisilino, et al. (1998).

For the next two homogeneous cases the direction of the axis of symmetry, $\boldsymbol{x_3^0}$, is chosen to be parallel to the crack plane, this is, coincident with the global directions x and z, respectively. For these cases the material elastic constants are chosen the same to those of the laminated used by Ariza and Dominguez (2004b). The five independent values of the coefficients of the tensor $\boldsymbol{C_{ij}}$ (see equation 3) are

$$C_{11} = 5.37 \text{ GPa},\ C_{12} = 1.34 \text{ GPa},\ C_{13} = 3.35 \text{ GPa},\ C_{33} = 251.168 \text{ GPa},\ \text{and } C_{44} = 5 \text{ GPa}. \quad (22)$$

The associated elastic properties are: E= 5 GPa, E'= 247.83 GPa, ν=0.245, ν'= 0.01 and μ'= 2.5. The material orientation is specified for each subdomain by means of the angles $(\boldsymbol{\alpha, \beta, \gamma})$ which define the orientation of $\boldsymbol{x_3^0}$, the material axis of symmetry, with respect to the global coordinate system $(\boldsymbol{x, y, z})$. In this way, for the material axis of symmetry oriented in the direction global direction x, the orientation angles are are 0°/90°/90°, while for the material axis of symmetry oriented in the global direction z, the angles are 90°/90°/0°.

Computed results along the crack front are presented in Figure 10. In other to compare with other results, data in Figure 10 is presented in terms of normalized stress intensity factors, $\boldsymbol{K_I/K_0}$, where $\boldsymbol{K_0 = \sigma\sqrt{\pi a}}$. To compute the stress intensity factors from the J results, the problem was assimilated to a two-dimensional one in the xy plane. Stress intensity factors were computed from the J results using the expressions (see Chu and Hong, 1990),

$$J_1 = a_{11}K_I^2 + a_{12}K_IK_{II} + a_{22}K_{II}^2 \quad (23)$$
$$\text{and } J_2 = b_{11}K_I^2 + b_{12}K_IK_{II} + b_{22}K_{II}^2,$$

where the coefficients a and b depend on the elastic material properties and the material orientation. The coefficients $\boldsymbol{a_{12}}$, $\boldsymbol{a_{22}}$ and the three coefficients $\boldsymbol{b}$ are zero when one of the principal axes of the material is parallel to the crack plane. Thus, for the cases considered in this work

$$J_1 = a_{11}K_I^2. \quad (24)$$

The values for the coefficient $\boldsymbol{a_{11}}$ as a function of the ratio between the Young modulus in the xy plane, $\boldsymbol{E_x/E_y}$, are reported in Table 1.

It can be seen in Figure 10 that with the only exceptions of the regions next to the lateral faces of the specimen (say, $\boldsymbol{|z/t| > 0.45}$) where the boundary layer effect takes place, the stress intensity factor value is nearly constant along the crack front. Also plotted in Figure 10 there are two sets of results computed using a two-dimensional high-resolution finite element model. The finite element model was solved using Abaqus (2009), and it was discretized using a fine regular mesh consisting of 9,600 8-node biquadratic, plane stress elements (CPS8R). The stress intensity factors were computed using an Abaqus built-in facility. The resultant normalized stress intensity factors are $\boldsymbol{K_I/K_0 = 1.124}$ and $\boldsymbol{K_I/K_0 = 1.184}$ for the material axis of symmetry oriented in the global directions x and z, respectively. The difference between the BEM and FEM results is less than 2%.

The final case consists in a heterogeneous plate with the axis of symmetry of the material oriented in the global directions z and y for the subdomains I and II, respectively; this is, 90°/90°/0° for the subdomain I and 90°/0°/90° for the subdomain II. The material elastic properties are the same of the previous cases. Computed results are presented in Table 2. The results are normalized with respect to $\boldsymbol{J_0 = \sigma^2\pi a/E'}$. It can be seen that J value is nearly constant along the complete crack front. Besides, the path independence is found excellent with a standard deviation of around 5% for the results computed using the domains with radii $\boldsymbol{r/a \geq 0.20}$. The only exceptions are the positions next to the lateral face of the specimen, where the

boundary layer effect takes place and the applicability of the *J*-integral is not strictly valid. The smallest integration domains with $\boldsymbol{r/a = 0.10}$ do not provide accurate results. This is attributed to the fact that these domains are discretized using a single cell in the radial direction. Similar behaviours were found in previous works by the authors (see for example Cisilino et al., 1998 and Ortiz and Cisilino, 2005).

7.2 Bimaterial laminate with an edge interface crack

It is considered in this example the analysis of an edge crack in a bimaterial laminate. The model geometry and discretization are depicted in Figure 11. Model dimensions are: crack length a=10 mm, specimen width b=4a, height h=a and thickness $2t$=1.5a. Material properties are the same used by Ariza and Dominguez (2004b) and reported in Equation (22) in the previous example. The discretization of the model is that illustrated in Figure 7, using 596 elements. Five rings of cells with normalized radii r/a = 0.05, 0.1, 0.15, 0.22 and 0.32 are accommodated around the crack front for the *J* computations. Five hundred and four cells are used in the construction of the integration domains.

The model was solved for a number of relative orientations of the axis of symmetry of the material in both subdomains. The computed results are reported in Figure 12. *J*-results in Figure 12 are normalized with respect to $\boldsymbol{J_0 = \sigma^2 \pi a / E'}$. It can be seen that when one of the principal axes of the material is specified perpendicular to the crack front direction for both subdomains, the *J*-integral results along the crack front are symmetric with respect to the specimen mid-plane (z/t=0). These are the cases for the results labelled 90°/90°/0°-90°/90°/0° and 0°/90°/90°-90°/90°/0° in the figure. On the other hand, when the orientation of the principal axes of the material are arbitrary in at least one of the two subdomains, the *J*-integral results along the crack front are not symmetric with respect to the specimen mid-plane. The extreme values for the *J*-integral are attained at the free surface.

7.3 A circumferential interface crack in a cylindrical bimaterial bar

The last example consists in a cylindrical bimaterial bar containing a circumferential crack subjected to remote axial tension σ, see Figure 13*a*. The radius of the bar is b=5a and its height h=24a, being a the crack depth. A total of 684 elements are employed in the model discretization. Four rings of cells with radii r/a = 0.25, 0.5, 0.75 and 1 are accommodated around the crack front for the *J* computations. Integration domains are constructed using 672 cells. The model discretization is illustrated in Figure 13*b*. Material properties are the same reported in Equation 22 for a previous example.

The problem was solved considering different material orientations. The results are reported in Figure 14. In every case the results are normalized with respect to $\boldsymbol{J_0 = \sigma^2 \pi a / E'}$. The first solution is for an isotropic homogeneous material and it was used with validation purposes. The *J* result is constant along the complete crack front. The difference between the computed result and that reported by Murakami and Okazaki (1976) is 5% (it is worth noting that the reported precision for the reference solution is 3%). The second solution is for a homogeneous transversely-isotropic case, with the material symmetry axis specified coincident with the direction y for both subdomains (results labeled 90°/0°/90°-90°/0°/90° in Figure 14). Once again, and as it was expected, the computed *J* values are constant along the complete crack front. In the third case the orientation of the material axis of symmetry are different in each subdomain: for the subdomain I the

material axis of symmetry is oriented in the z-direction, while for the subdomain II it is oriented in the y-direction (results labelled 90°/90/0°-90°/0°/90° in Figure 14). The J results exhibit a periodic variation along the crack front. Minimum values occur in the positions coincident with the direction of the z-axis, while the maximums are in the positions coincident with the direction of the x-axis. In the last case, the orientation of the material axis of symmetry is specified in the x-direction for both subdomains (results labelled 0°/90/90°-0°/90°/90° in Figure 14). As for the previous case, the J results exhibit a periodic variation along the crack front. However, in this case minimum values occur in the positions coincident with the direction of the x-axis, while the maximums are in the positions coincident with the direction of the z-axis.

8 Conclusions

A boundary element methodology for the analysis of three-dimensional interface cracks in transversely isotropic bimaterials has been presented in this paper. The analysis is addressed using a multidomain BEM formulation in order to account for the different material properties at both sides of the crack. The J-integral is computed along the crack front using the Energy Domain Integral (EDI) methodology. This is implemented as a post-processing technique, and so, it can be applied to the results from a particular model at a later stage. The implementation takes advantage of the efficiency of the boundary integral equation to directly obtain the required displacement derivatives, stress and strain fields from their boundary integral representations.

The efficiency and accuracy of the proposed implementation has been addressed by analysing a number of examples with straight and curved crack fronts. The computed results compared very well with those reported in the literature for benchmark problems. Besides, the implemented algorithm allowed studying the effect of the relative orientations of the materials on both sides of the crack on the J integral values.

Maximum errors and dependence of the computed results with the integration paths occur for surface cracks at the intersection of the crack front with a free surface. In this sense it is worth noting that the formulation of EDI methodology used in this work is based on the assumption that the near-crack tip fields asymptote to the plane strain fields along the crack front. But it turns out that this assumption does not hold at the intersection of the crack front and a free surface, and so the proposed methodology is not strictly applicable. This problem remains unsolved in this work. Following previous work (Cisilino and Ortiz, 2005), alternative approaches for the selection of the auxiliary function $\boldsymbol{q}$ for the implementation of the EDI could be explored to improve the accuracy of the computations.

Acknowledgements

This work has been partially supported by the Agencia Nacional de Promoción Científica y Tecnológica (ANPCyT) of Argentina through the grant PICT 2007 Nº 1154. J.E. Ortiz has been supported by the Programa Ramón y Cajal of the Spanish Ministry of Science and Innovation.

References

Abaqus 6.9-1 (2009). Dassault Systemes, Providence, RI, USA

Aliabadi M.H. (1996): Database of Stress Intensity Factors. *Computational Mechanics Publications*, Southampton, UK.

Aliabadi M.H. (1997). Boundary element formulations in fracture mechanics. *Applied Mechanics Review*, 50: 83-96.

Aliabadi M.H. (2002). *The Boundary Element Method, Volume II: Applications in Solids and Structures*. Wiley, Chichister, UK.

Anderson T.L. (2005). *Fracture Mechanics: Fundamentals and Applications*. Second Edition, CRC Press, Boca Ratón, USA.

Ariza M.P. and Dominguez J. (2004a). Dynamic BE analysis of 3-D cracks in transversely isotropic solids. *Computer Methods in Applied Mechanics and Engineering*, 193/9-11: 765-779.

Ariza M.P. and Dominguez J. (2004b). Boundary element formulation for 3D transversely isotropic cracked bodies. *International Journal for Numerical Methods in Engineering*, 60/4: 719-753.

Balderrama R., Cisilino A.P., Martinez M. (2006). BEM analysis of three-dimensional fracture problems using the energy domain integral. *ASME Journal of Applied Mechanics*, 73/6:959-969.

Balderrama R., Cisilino A.P., Martinez M. (2008). Boundary element analysis of three-dimensional mixed-mode thermoelastic crack problems using the interaction and the energy domain integrals. *International Journal for Numerical Methods in Engineering*, 74/2: 294-320.

Boniface V. and Banks-Sills L. (2002). Stress intensity factors for finite interface cracks between a special pair of transversely isotropic materials. *ASME Journal of Applied Mechanics*, 69/3: 230-239.

Bowie, O.L.; Freese, C.E. (1972) Central crack in plane orthotropic rectangular sheet. *International Journal of Fracture Mechanics*, vol. 8/1, pp. 49-58.

Chen C-S, Chen C-H and Pan E. (2009). Three-dimensional stress intensity factors of a central square crack in a transversely isotropic cuboid with arbitrary material orientations. *Engineering Analysis with Boundary Elements*, 33: 128– 136

Chow W. T. and Atluri S. N. (1998). Stress intensity factors as the fracture parameters for delamination crack growth in composite laminates. Computational Mechanics, 21: 1-10.

Chu S.J. and Hong C.S. (1990). Application of the J_k integral to mixed mode crack problems for anisotropic composite laminates. *Engineering Fracture Mechanics*, 35/6:1093-1103.

Cisilino A.P., Aliabadi M.H. and Otegui J.L. (1998). Energy domain integral applied to solve centre and double-edge crack problems in three dimensions. *Theoretical and Applied Fracture Mechanics*, 29:181-194.

Cisilino A.P. and Aliabadi M.H. (1999). Elastoplastic BEM implementation of the energy domain integral for the analysis of 3D fracture problems. *International Journal of Fracture*, 96:229-245.

Freed Y. and Banks-Sills L. (2005). A through interface crack between a ±45◦ transversely isotropic pair of materials. *International Journal of Fracture* , 133: 1–41.

Gibson R.F. (2007). *Principles of Composite Material Mechanics*. CRC Press, London.

He W.J., Lin D.S. and Ding, H.J. (1994). A boundary element for crack analysis at a bimaterial interface. *Engineering Fracture Mechanics*, 49/3:405-410.

Lachat J.C. and Watson J.O. (1976). Efective numerical treatment of boundary integral equations: a formulation for three-dimensional elastostatics. *International Journal for Numerical Methods in Engineering*, 10: 991-1005.

Loloi M. (2000). Boundary integral equation solution of three-dimensional elastostatic problems in transversely isotropic solids using closed-form displacement fundamental solutions. *International Journal for Numerical Methods in Engineering*, 48: 823-842.

Mao R. and Sun G. (1995). A study of the interaction between matrix crack and matrix-fibre interface. *Engineering Fracture Mechanics*, 51/3: 469-477.

Moran B. and Shih C.F. (1987). A general treatment of crack tip contour integrals. International *Journal of Fracture*, 35/4: 295-310.

Murakami Y. and Okazaki Y. (1976). A simple procedure for the accurate determination of stress intensity factors by finite element method. *Trans. Japan Soc. Mech. Engrs.*, 42/364: 3679-3687

Natha R. and Moran B. (1993). Domain integrals for axisymmetric interface crack problems. *International Journal of Solids & Structures*, 30/15: 2027-2040.

Nikishkov G.P. and Atluri S.N. (1987). Calculation of fracture mechanics parameters for an arbitrary three-dimensional crack by the equivalent domain integral method. *International Journal of Numerical Methods in Engineering*, 24/9:1801-1821.

Omer N. and Yosibash Z. (2008). Edge singularities in 3-D elastic anisotropic and multi-material domains. *Computer Methods in Applied Mechanics and Engineering*, 197: 959-978.

Ortiz J.E. and Cisilino A.P. (2005). Boundary element method for J-integral and stress intensity factor computations in three-dimensional interface cracks. *International Journal of Fracture*, 133:197-222.

Pan Y. and Chou, T. (1976). Point solution for an infinite transversely isotropic solid. *Journal of Applied Mechanics*, 98: 608-612.

Raju I.S. and Newman J.C. (1977). Three-dimensional finite-element analysis of fnite-thickness fracture specimens. *Technical Report NASA TN D-8414*.

Rice J.R. (1968). A path independent integral and the approximate analysis of strain concentration by notches and cracks. *ASME Journal of Applied Mechanics*, 379-386.

Sáez A., Ariza, M.P. and Dominguez J. (1997) Three-dimensional fracture analysis in transversely isotropic solids. *Engineering Analysis with Boundary Elements*, 20/4: 287-298.

Saliva R., Vénere M.J., Padra C., Taroco E. y Feijoó R.A. (2000). Shape sensitivity analysis and energy release rate of planar cracks embedded in three-dimensional bodies. *Computer Methods in Applied Mechanics and Engineering*, 188: 649-664.

Shah P.D., Tan C.L. and Wang X. (2006). Evaluation of T-stress for an interface crack between dissimilar anisotropic materials using the boundary element method. *Computer Modeling in Engineering & Science*, 13/3:185-197.

So W.M.G., Lau K.J. and Ng S.W. (2004). Determination of stress intensity factors for interfacial cracks using the virtual crack extension approach. *Computer Modeling in Engineering & Science*, 5/3:189-200.

Synge J.L.; Schild A. (1978). Tensor Calculus, Dover Publications, New York.

Tan C.L. and Gao Y.L. (1990). Treatment of bimaterial interface crack problems using the boundary element method. *Engineering Fracture Mechanics*, 36: 919-932.

Távara L., Ortiz J.E., Mantic, V. and París, F. (2008). Unique real-variable expressions of displacement and traction fundamentals solutions covering all transversely isotropic elastic materials for 3D BEM. *International Journal for Numerical Methods in Engineering*, 74:776-798.

Távara L., Mantic V., Ortiz J.E. and París F. (2009). Unique real-variable expressions of the integral kernels in the stress hypersingular boundary integral equation covering all transversely isotropic elastic materials for 3D BEM. *Submitted to the International Journal for Numerical Methods in Engineering*.

Ting T.C.T. (1996). *Anisotropic Elasticity: Theory and Applications*. Oxford University Press, Oxford, UK.

Appendix A

Non-zero components of the tensor $\boldsymbol{H}(\hat{\boldsymbol{x}})$:

$$\boldsymbol{H_{11}} = \frac{\mathbf{1}}{\mathbf{C_{66}}\boldsymbol{\beta_3}} + \frac{\mathbf{C_{44}}\boldsymbol{c^2} + \mathbf{C_{33}}\boldsymbol{s^2}}{\mathbf{C_{11}C_{44}}\boldsymbol{gh}} - \frac{\boldsymbol{f}}{\boldsymbol{\xi}} \tag{A1}$$

,

$$\boldsymbol{H_{22}} = \frac{\mathbf{1}}{\mathbf{C_{11}}\boldsymbol{g}} + \frac{\boldsymbol{f}}{\boldsymbol{\xi}}, \tag{A2}$$

,

$$\boldsymbol{H_{33}} = \frac{\mathbf{1}}{\boldsymbol{gh}}\left\{\frac{\boldsymbol{h}+\boldsymbol{c^2}}{\mathbf{C_{44}}} + \frac{\boldsymbol{s^2}}{\mathbf{C_{11}}}\right\}, \tag{A3}$$

$$H_{13} = \frac{(\mathrm{C}_{13} + \mathrm{C}_{44})sc}{\mathrm{C}_{11}\mathrm{C}_{44}gh}, \tag{A4}$$

$$\beta_3 = \left\{\frac{\mathrm{C}_{44}c^2 + \mathrm{C}_{33}s^2}{\mathrm{C}_{66}}\right\}^{1/2}, \tag{A5}$$

$$h = \left\{c^4 + \frac{\eta s^2 c^2}{\mathrm{C}_{11}\mathrm{C}_{44}} + \frac{\mathrm{C}_{33}s^4}{\mathrm{C}_{11}}\right\}^{1/2}, \tag{A6}$$

$$g = \left\{2(h + c^2) + \frac{\eta s^2}{\mathrm{C}_{11}\mathrm{C}_{44}}\right\}^{1/2}, \tag{A7}$$

$$\xi = g(h + g\beta_3 + \beta_3^2), \tag{A8}$$

$$\eta = \mathrm{C}_{11}\mathrm{C}_{33} - \mathrm{C}_{13}^2 - 2\mathrm{C}_{13}\mathrm{C}_{44}, \tag{A9}$$

where $= \cos\phi = x_3/r$, $s = \sin\phi = r_{12}/r$ and the angle ϕ is indicated in Figure 4.

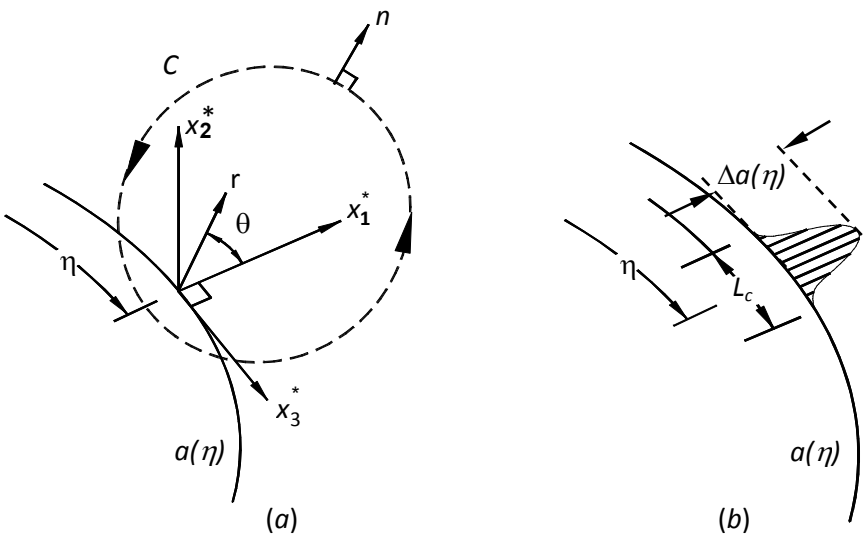

Figure 1: (*a*) Definition of the local orthogonal Cartesian coordinates at point η on the crack front, (*b*) Virtual crack front advance.

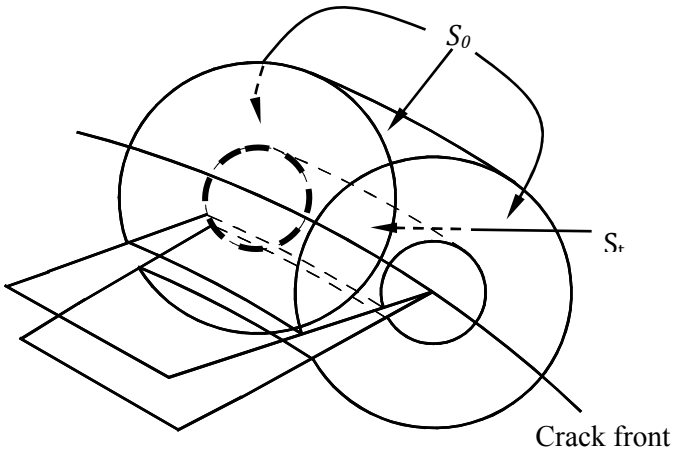

Figure 2: Tubular domain surrounding a segment of the crack front.

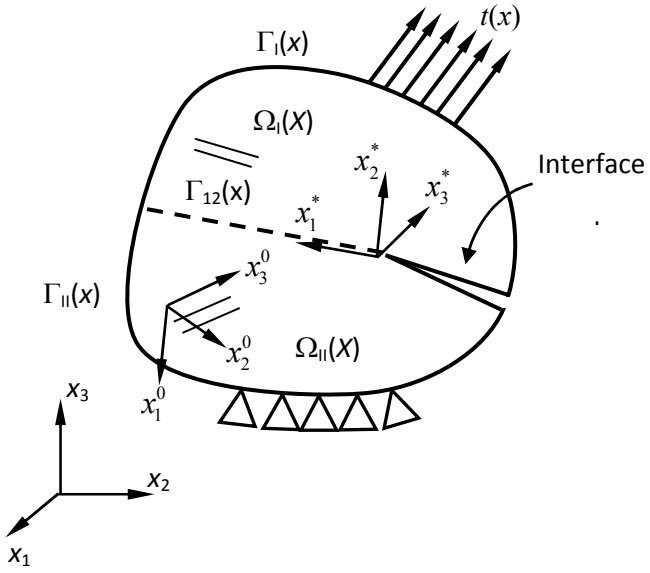

Figure 3: Schematic two-dimensional representation of the multi-domain BEM model with an interface crack.

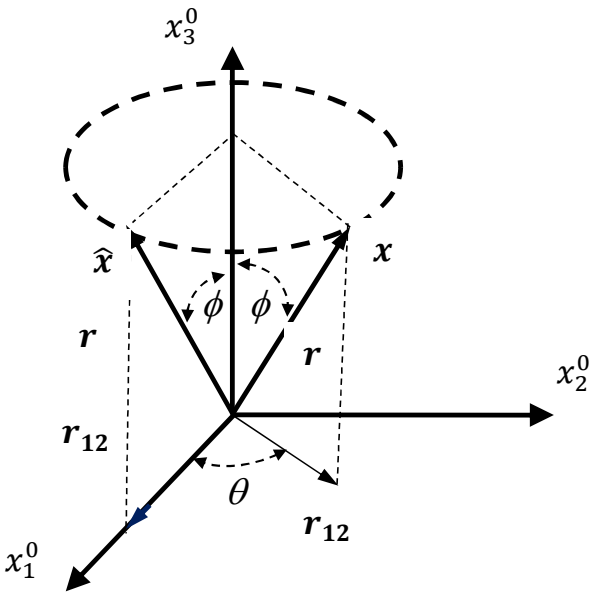

Figure 4: Point **x** and $\hat{\mathbf{x}}$ associated with a transversely isotropic material.

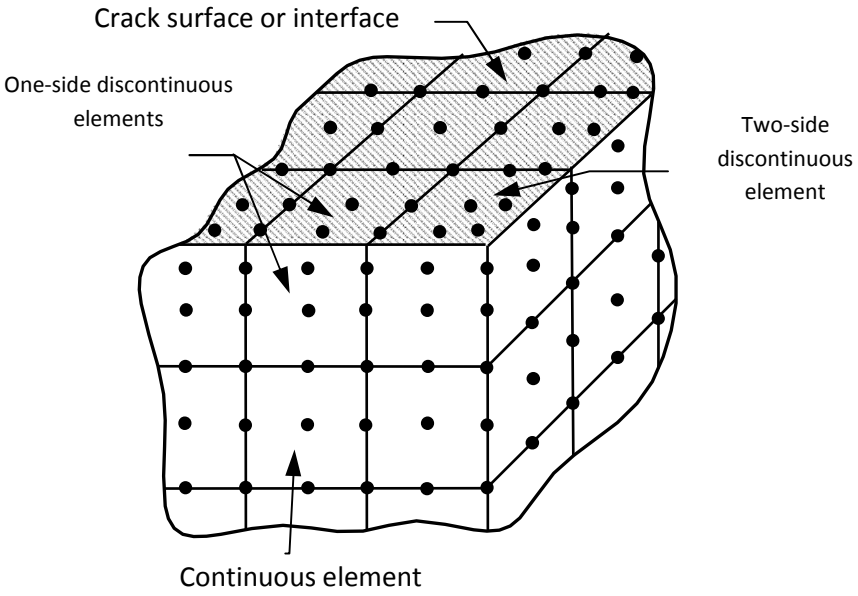

Figure 5: Model discretization strategy using continuous and

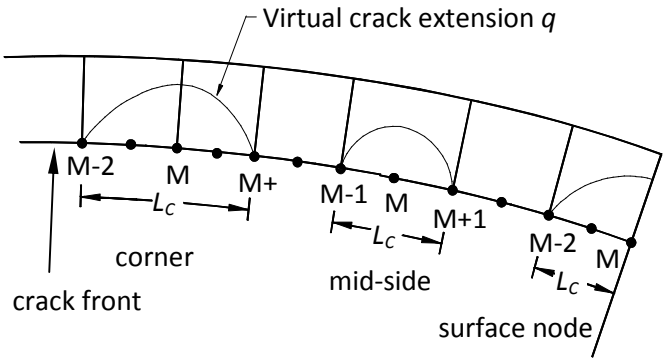

Figure 6: Schematic of the crack front region illustrating the virtual crack extensions for a corner node, a mid-node and a surface node.

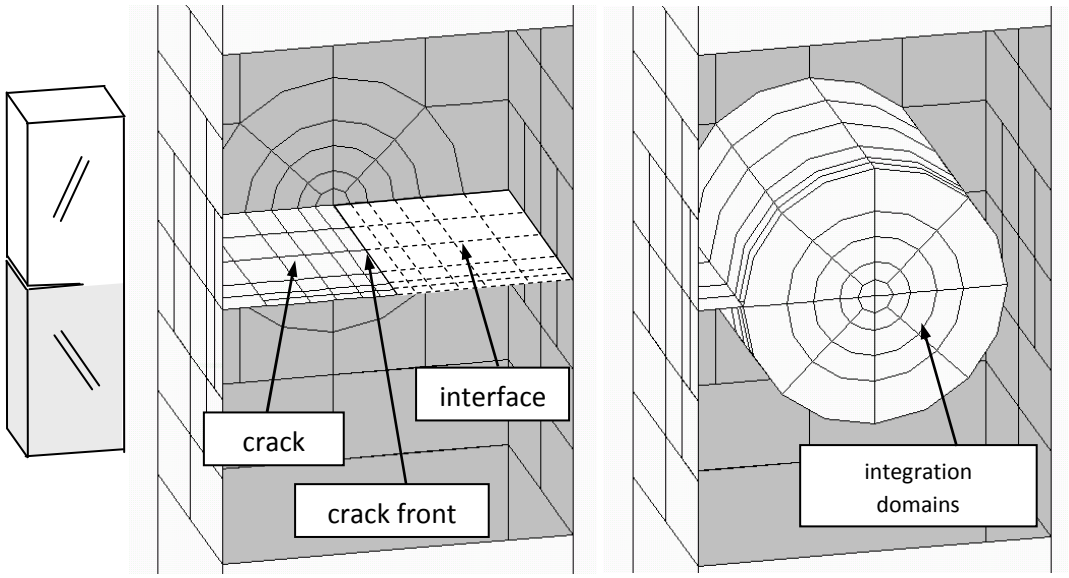

Figure 7: (*a*) Problem geometry, (*b*) Boundary Element discretization,

(*c*) Integration domains.

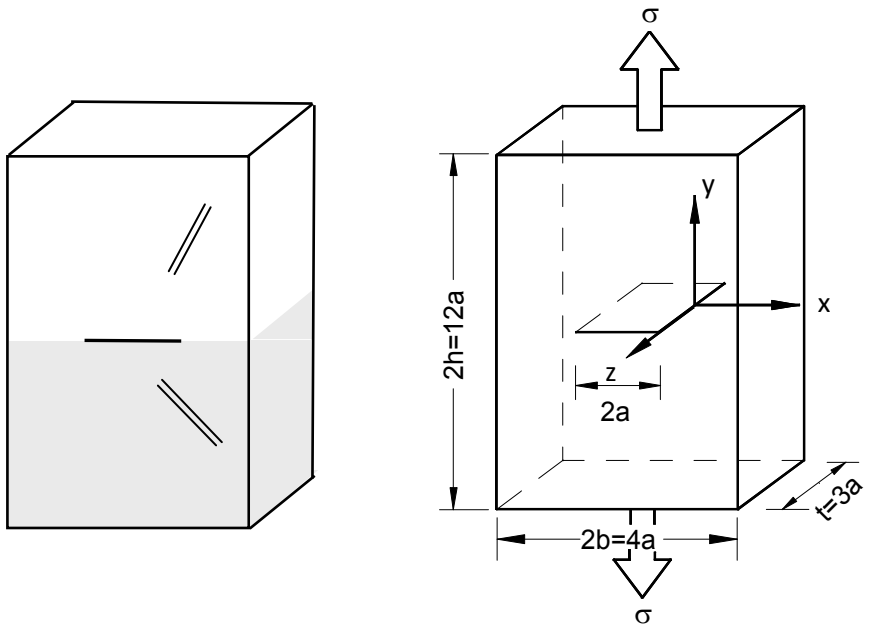

(a) *(b)*

Figure 8: (*a*) Schematic representation of the thick tension plate with a centre interface crack, (*b*) Model dimensions.

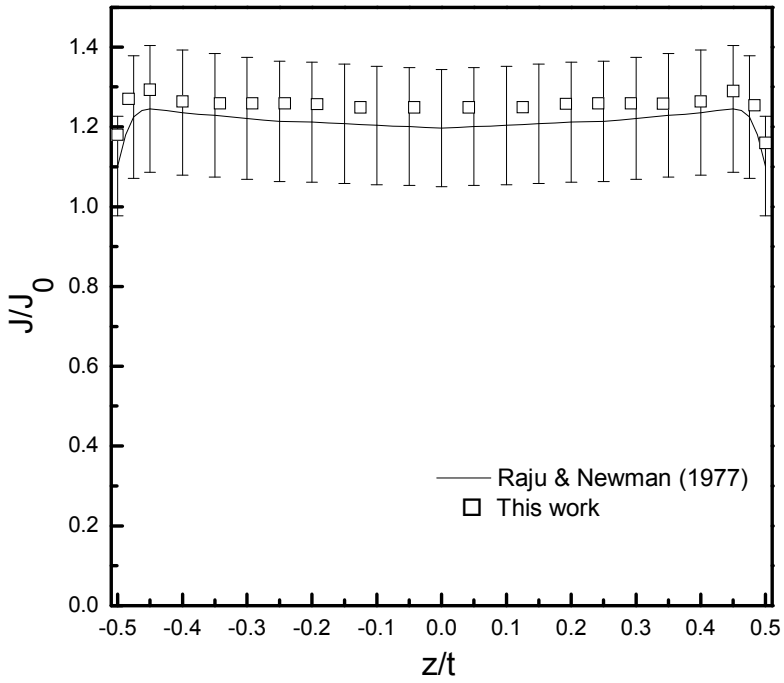

Figure 9: Normalized *J*-integral results along the crack front for the homogeneous isotropic centre crack specimen.

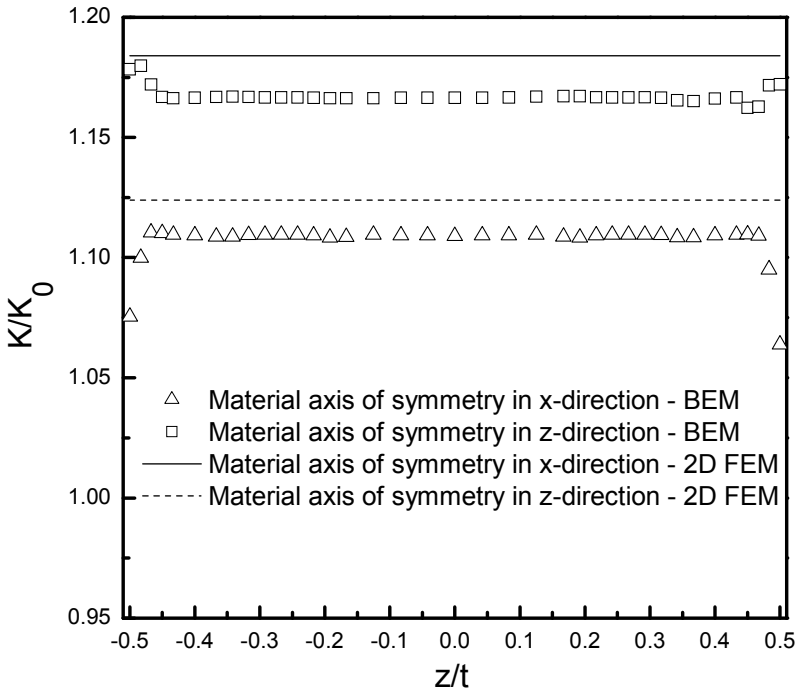

Figure 10: Normalized *SIF* results along the crack front for the homogeneous transversely-isotropic centre crack specimen.

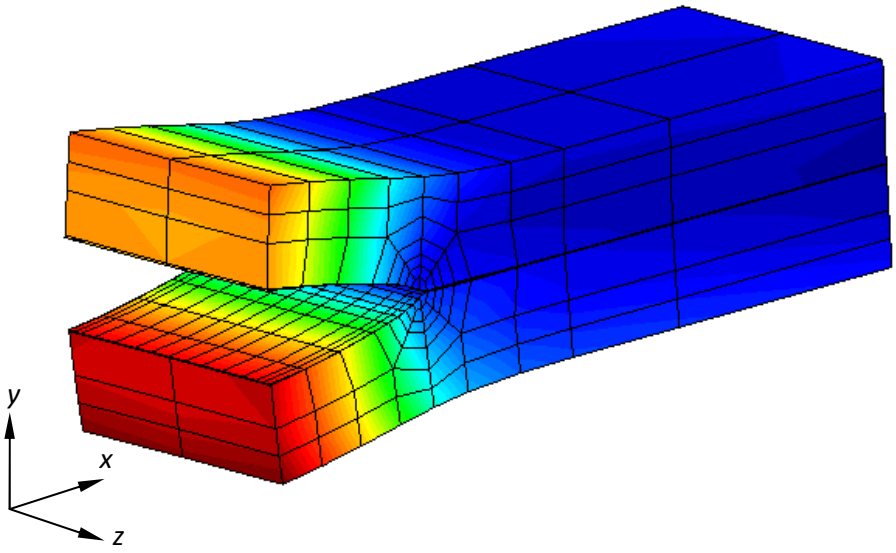

Figure 11: Bimaterial laminate with an edge crack (deformed geometry)

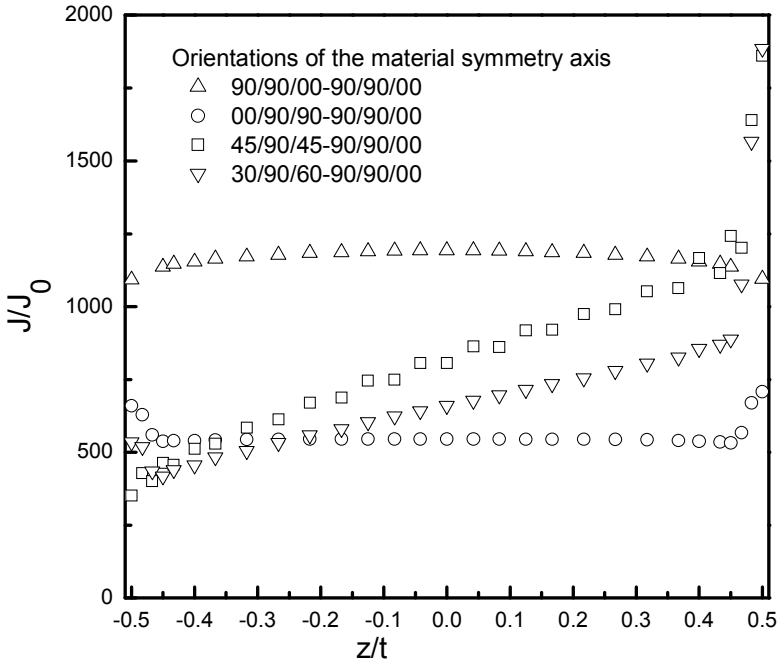

Figure 12: Normalized *J*-integral results along the crack front of the edge crack in the ply.

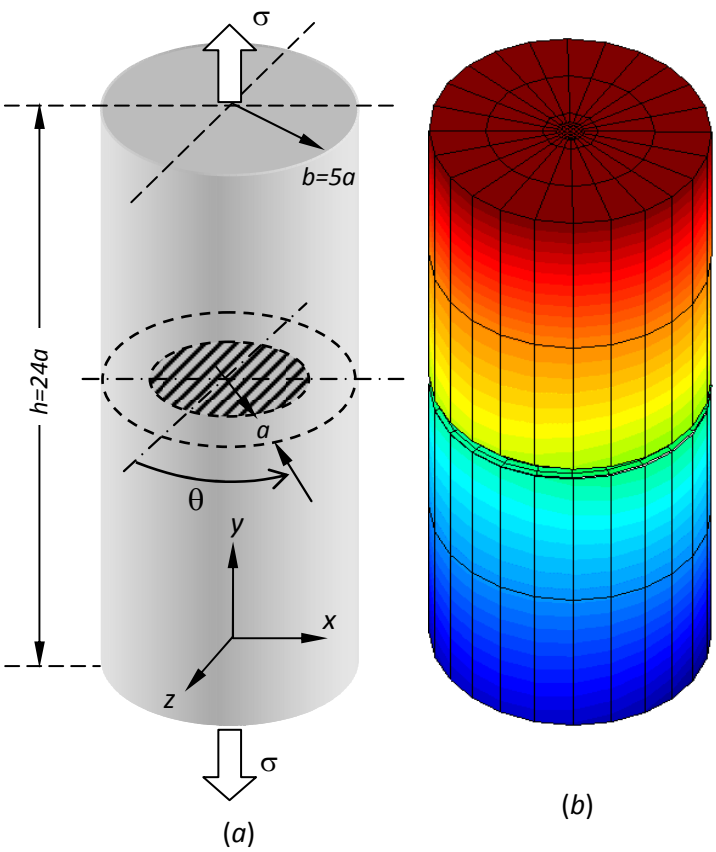

Figure 13: External circumferential interface crack in a cylindrical bimaterial bar, (*a*) model geometry and dimensions, (*b*) model discretization (deformed mesh)

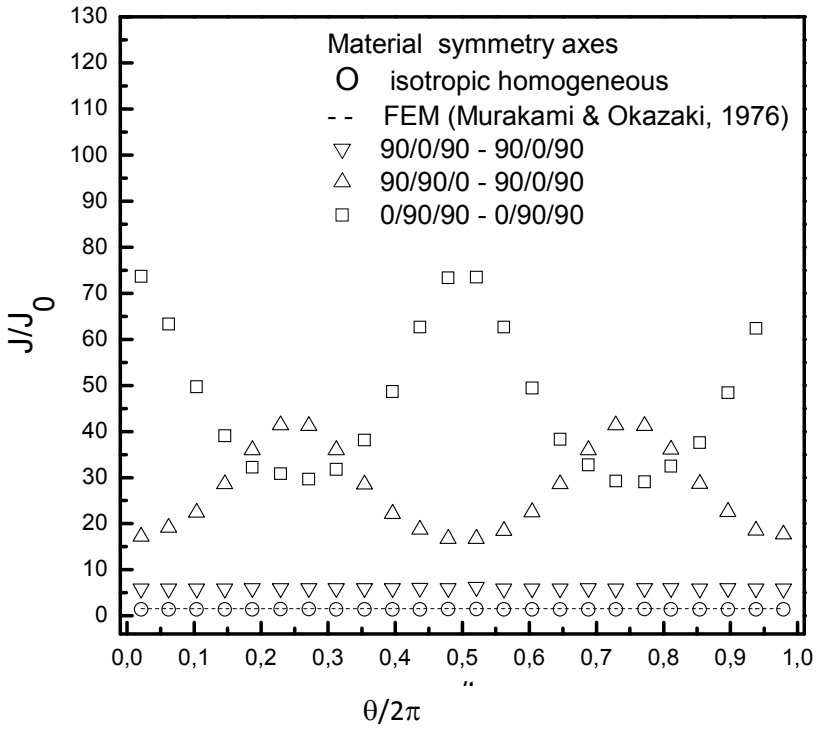

Figure 14: Normalized *J*-integral results along the crack front of the circumferential crack in the biomaterial bar.

Table 1: Resulting values for the coefficients a_{11} and Young Modulus ratios used to compute stress intensity factors from the J results.

Case	a_{11}	E_x/E_y
Material symmetry in x- direction	$0.112\ 10^{-9}$	49.57
Material symmetry in z- direction	$0.2\ 10^{-9}$	1

Table 2: Normalized J-integral results for the heterogeneous plate as a function of the integration domain size. The results for the smallest integration domains, r/a=1 (shaded column in the table) are excluded for the computation of the average value and the STD.

z/t	r/a					Average	STD
	0.10	0.20	0.30	0.44	0.64		
0.000	25.6382	30.4503	30.7658	30.7658	30.6081	30.5613	0.49
0.042	25.6382	30.4503	30.7658	30.7658	30.6081	30.5566	0.49
0.083	25.6382	30.4503	30.7658	30.7658	30.6081	30.5512	0.49
0.125	25.6382	30.4503	30.7658	30.7658	30.6081	30.5452	0.49
0.167	25.6382	30.4503	30.7658	30.7658	30.6081	30.5384	0.49
0.192	25.6382	30.4503	30.6869	30.7658	30.6081	30.5306	0.44
0.217	25.6382	30.4503	30.6869	30.7658	30.6081	30.5231	0.44
0.242	25.6382	30.4503	30.6869	30.7658	30.6081	30.5144	0.44
0.267	25.6382	30.4503	30.6869	30.7658	30.6081	30.5041	0.44
0.292	25.6382	30.4503	30.6869	30.7658	30.6081	30.4917	0.44
0.317	25.6382	30.3714	30.6869	30.6869	30.5292	30.4766	0.50
0.342	25.6382	30.3714	30.6081	30.6869	30.4503	30.4651	0.47
0.367	25.6382	30.3714	30.6081	30.6081	30.4503	30.4559	0.39
0.400	25.5593	30.3714	30.6081	30.6081	30.4503	30.4470	0.39
0.433	25.5593	30.2925	30.6081	30.6081	30.4503	30.4345	0.50
0.450	25.5593	30.2925	30.5292	30.6081	30.4503	30.4207	0.44
0.467	25.4804	30.2925	30.6869	30.7658	30.6869	30.4043	0.70
0.483	25.0071	29.9770	30.7658	31.1603	31.2391	30.3024	1.91
0.500	23.5871	28.5570	29.7403	30.3714	30.6081	29.8192	3.08

Computational Methods in Fracture Mechanics
doi:10.4028/www.scientific.net/KEM.454

Boundary Element Analysis of Three-Dimensional Interface Cracks in Transversely Isotropic Bimaterials Using the Energy Domain Integral
doi:10.4028/www.scientific.net/KEM.454.47